

# Soft $\gamma$ -ray selected giant radio galaxies: an update

L. Bassani,<sup>1\*</sup> F. Ursini<sup>2</sup>, A. Malizia<sup>1</sup>, G. Bruni<sup>3</sup>, F. Panessa<sup>3</sup>, N. Masetti<sup>1,5</sup>, I. Saviane<sup>4</sup>,  
L. Monaco<sup>5</sup>, T. Venturi<sup>6</sup>, D. Dallacasa<sup>7,6</sup>, A. Bazzano<sup>3</sup>, and P. Ubertini<sup>3</sup>

<sup>1</sup> *INAF/OAS Bologna, Via P. Gobetti 101, I-40129 Bologna, Italy*

<sup>2</sup> *Dipartimento di Matematica e Fisica, Università Roma Tre, via della Vasca Navale 84, I-00146 Roma, Italy*

<sup>3</sup> *INAF/IAPS Roma, Via Fosso del Cavaliere 100, I00133 Roma, Italy*

<sup>4</sup> *European Southern Observatory, Alonso de Cordova, 3107, Santiago, Chile*

<sup>5</sup> *Departamento de Ciencias Físicas, Universidad Andrés Bello, Fernández Concha 700, Las Condes, Santiago, Chile.*

<sup>6</sup> *INAF/IRA Bologna, Via P. Gobetti 101, I-40129 Bologna, Italy*

<sup>7</sup> *Dipartimento di Fisica e Astronomia, Università di Bologna, Via Gobetti 93/2, 40129 Bologna, Italy*

Accepted XXX. Received YYY; in original form ZZZ

## ABSTRACT

We present an update on the sample of soft gamma-ray selected giant radio galaxies (GRGs) extracted from INTEGRAL/IBIS and Swift/BAT surveys; it includes 8 new sources and one candidate object. In the new sample all, but one source, display FR II radio morphologies; the only exception is B21144+35B which is an FR I. The objects belong to both type 1 and 2 AGN optical classes and have redshifts in the range 0.06–0.35, while the radio sizes span from 0.7 to 1 Mpc. In this study, we present for the first time two objects that were never discussed as GRGs before and propose a new candidate GRG. We confirm the correlation between the X-ray luminosity and the radio core luminosity found for other soft gamma-ray selected GRGs and expected for AGNs powered by efficient accretion. We also corroborate previous results that indicate that the luminosity of the radio lobes is relatively low compared with the nuclear X-ray emission. This supports the idea that the nucleus of these GRGs is now more powerful than in the past, consistent with a restarting activity scenario.

**Key words:** galaxies: active – gamma-rays: galaxies – radio continuum: galaxies

## 1 INTRODUCTION

A small fraction of radio galaxies exhibits exceptional linear extents, i.e. above 0.7 Mpc (for  $H_0 = 71 \text{ km s}^{-1} \text{ Mpc}^{-1}$ ). Defined as Giant Radio Galaxies (GRGs), these objects represent the largest and most energetic single entities in the Universe and are of particular interest as extreme examples of radio source development and evolution. Detailed studies of the age of some GRGs suggest that their lobes formed during tens, possibly hundreds, of Myr (see e.g. Bruni et al. 2020 and references therein); with such long period of activity they are the ideal targets to study the duration of the radio phase in AGN and its duty cycle. GRGs are also interesting for many aspects of astrophysical research: as unique laboratories where to study particle acceleration processes and understand cosmic magnetism (Kronberg et al. 2004; Stuardi et al. 2020), to study the formation of large-scale structures and also to probe the Warm-Hot Intergalactic Medium interacting with the magnetized relativistic plasma (Malarecki et al. 2013). Recently the study of GRGs has gained momentum thanks to LOFAR observations, which allow to discover new objects (Dabhade et al. 2020b) providing at the same time interesting insights into their nature (Dabhade et al. 2020a).

Starting from 2002, the soft gamma-ray sky has been surveyed by INTEGRAL/IBIS and subsequently by Swift/BAT at energies

above 10 keV. Up to now various all sky catalogues have been released revealing a large population of active galactic nuclei. More specifically, around 6–8% of these soft gamma-ray selected AGNs display a double lobe morphology typical of radio galaxies (Bassani et al. 2016). What is intriguing and particularly interesting is that a substantial fraction (25%) of these radio galaxies have giant radio structures: considering that the overall fraction of giants in samples of radio galaxies is much lower ( $\sim 6\%$  in the 3CR catalogue, Ishwara-Chandra & Saikia 1999 and  $\sim 8\%$  among LOFAR objects, Dabhade et al. 2020b), the fraction found in soft gamma-ray surveys is impressive, and suggests a tight connection between the nuclear/accretion properties of the AGN and the radio source size. At the moment 14 GRGs<sup>1</sup> have been already found within INTEGRAL/IBIS and Swift/BAT surveys (Bassani et al. 2016), but these databases are constantly being updated allowing the identification of new soft gamma-ray selected objects. After their initial finding, Bassani et al. (2016) put a large observational effort to study the first soft gamma-ray selected sample of 14 GRGs, finding evidence of restarting radio activity in almost every object given that some GRGs host a young radio core (Giga Hertz/High Frequency Peaked or GPS/HFP, Bruni et al. 2019) while others display a double-double and/or X-shaped morphology (Bruni et al. 2020). Note that the radio-emitting electrons in GP-

<sup>1</sup> See GRACE at <https://sites.google.com/inaf.it/grace/home>, for information on this first sample

\* Contact e-mail: [loredana.bassani@inaf.it](mailto:loredana.bassani@inaf.it)

S/HFP sources usually have a radiative age of a few kyr, while the Mpc-scale structure of GRGs usually takes tens/hundreds of Myr to develop. Furthermore, a double-double morphology implies a source showing two pairs of lobes around a common core while an X shaped one could be the result of a drastic jet axis flip producing new lobes with different orientation on top of relic ones (but see the case of NCG326, [Hardcastle et al. 2019](#)): overall both morphologies can be taken as signs of multiple episodes of activity. Our team also found that one GRGs underwent a jet axis change of about 90 degrees and is now pointing towards us like a blazar ([Hernández-García et al. 2017](#)); another source was found to be enclosed in a diffuse radio emitting cocoon, relic of a previous active phase ([Bruni et al. 2020](#)). Overall these results imply that soft gamma-ray selected GRGs are extremely interesting objects and important laboratories where to study AGN duty cycle.

In this paper, we report an update to the original list of soft gamma-ray selected GRGs; this new sample lists 8 more sources plus a candidate one, including 2 (possibly 3 if the candidate is confirmed) new giant radio galaxies. For each radio galaxy we measured the largest angular size (LAS) in arcsec and then calculated the corresponding projected linear size in Mpc at the source's redshift assuming standard cosmological parameters ( $H_0=71 \text{ km s}^{-1} \text{ Mpc}^{-1}$ ,  $\Omega=0.27$ ,  $\Omega_\Lambda=0.73$ ) consistent with our previous work ([Bassani et al. 2016](#)).

The radio as well as the high energy properties of the sample are also presented and discussed.

## 2 RESULTS

Following the release of new INTEGRAL/Swift AGN surveys, we are now able to update the list of soft gamma-ray GRGs with respect to our previous work ([Bassani et al. 2016](#)). For INTEGRAL/IBIS, we consider the sample of 107 new AGN discussed by [Malizia et al. \(2016\)](#) with the addition of 43 new objects reported by [Mereminskiy et al. \(2016\)](#) in the deep extragalactic surveys of M81, LMC and 3C273/Coma regions and those reported by [Krivonos et al. \(2017\)](#) in the Galactic Plane Survey after 14 years of INTEGRAL observations. For Swift/BAT we use the 105 month catalogue of [Oh et al. \(2018\)](#) considering only the AGN of all types and the sources of Unknown class (U1, U2 and U3) listed among the 422 extra detections reported with respect to the 70 months catalogue. U type objects did not have a firm optical counterpart at the time of the survey release due to the lack of X-ray data (U3) or having X-ray measurements but not an X-ray detection (U2) or a credible optical (U1) association.

Following our previous work, we examined the radio structure of each new AGN reported in the high energy catalogues or found through this work (see following discussion and Appendix A), by inspecting images from the NRAO VLA Sky Survey (NVSS, [Condon et al. 1998](#)), the VLA FIRST Survey (FIRST, [White et al. 1997](#)), the Sydney University Molonglo Sky Survey (SUMSS, [Mauch et al. 2003](#)), or considering data already available in the literature. For objects located north of declination -40 degrees we used 1.4 GHz maps from the NVSS, the accuracy of which is  $\sim 10''$ , i.e. 1/4 of the survey angular resolution of  $45''$ ; the survey rms noise is 0.45 mJy/beam. We also complemented such information with images at the same frequency from the FIRST survey whose smaller point spread function or PSF ( $5''$ ) allows better accuracy (of the order of  $1.5''$ ) and an average rms noise of 0.15 mJy/beam. For particularly interesting sources (see following sections), we also inspected maps from the recent VLA Sky Survey (VLASS Epoch 1, [Lacy et al. 2020](#)) which provides a much better resolution ( $2.5''$ ) at slightly higher frequencies and a typical rms noise of 0.12 mJy/beam. For

objects located south of -40 degrees in declination, we used 0.8 GHz SUMSS images; here the accuracy is worse, both in terms of angular resolution ( $\sim 20''$ , as a result of a wider PSF) and rms noise (around 1 mJy/beam).

All together we inspected around 570 images to uncover those sources which display a double lobe morphology typical of radio galaxies of both FR I and FR II classes<sup>2</sup>.

In this way, we extracted a list of 7 new soft gamma-ray selected GRGs, plus 1 object, SWIFT J0225.8+5946, which is large in extent (10.5 arcmin) but for which we still lack a redshift measurement, so that we cannot confirm at this stage if the source is a GRG or not. We note however that for any redshift above 0.06 the source will be classified as a GRG.

We further add to the list a previously reported radio galaxy, IGR J13107-5626 ([Bassani et al. 2016](#)), for which we were able to obtain for the first time an optical spectrum and therefore estimate the source's class and redshift; details of the optical spectroscopy are reported in section 3.2 and in Appendix B. At the measured redshift, the source can now be classified as a new giant radio galaxy, since its size is just above 0.7 Mpc.

The new objects presented here and to be added to the sample of GRGs in [Bassani et al. \(2016\)](#) are all listed in Table 1. All sources are new Swift/BAT gamma-ray detections with the exception of IGR J13107-5626 also seen by INTEGRAL/IBIS and B2 1144+35B which instead is only listed in the INTEGRAL catalogue and has already been studied in some detail by our team ([Bruni et al. 2019, 2020](#)).

Two objects in the sample, SWIFT J1153.9+5848 and SWIFT J1503.7+6850, were classified as Unknown (U1 and U3 respectively) in the BAT survey. We have been able to update their class, and thanks to recent Swift/XRT observations, found the X-ray/radio counterpart of each of these two objects. In particular, we analysed all archival XRT pointings and stacked them together to enhance the signal to noise ratio. The restricted soft X-ray error box allowed the subsequent association of both objects to radio galaxies of large extension: RGB J1153+585 and 4C+69.18 for SWIFT J1153.9+5848 and SWIFT J1503.7+6850 respectively (see Appendix A for details on the X-ray data analysis and results).

We also checked that for the remaining 7 objects, the X-ray/optical counterpart reported in the corresponding high energy survey was the correct one. For this purpose we examined available observations from the Swift/XRT archive for SWIFT J0632.1-5404, SWIFT J0636.5-2036, SWIFT J0801.7+4764, B2 1144+35B, IGR J13107-5626 and SWIFT J0225.8+5946 and a Chandra pointing for SWIFT J1238.4+5349; the data analysis relative to all these objects is also reported in Appendix A.

All but one source in Table 1 display an FR II radio morphology; the only exception is B2 1144+35B which belongs to the FR I class. The sample includes local AGNs ( $z \leq 0.35$ ) of different optical classes with type 1 and 2 objects being equally represented; we note that two objects have redshift above 0.3, i.e. slightly higher than those reported by [Bassani et al. \(2016\)](#) indicating that as soft gamma-ray surveys improve their sensitivities (typically by a factor 1.4-1.5 with respect to our previous work), GRGs at higher  $z$  are detected. The soft gamma-ray luminosities are within the range observed by [Bassani et al. \(2016\)](#) for the previous sample of 14 GRGs, while the radio sizes span from 0.7 to 1 Mpc.

<sup>2</sup> FR I are sources whose luminosity decreases as the distance from the central galaxy or quasar host increases, while FR II sources exhibit increasing luminosity in the lobes ([Fanaroff & Riley 1974](#))

**Table 1.** New soft gamma-ray selected Giant Radio Galaxies. The columns from 1 to 10 report the source name (soft gamma-ray plus another from SIMBAD), redshift, optical class, radio morphology, 14–195 keV soft gamma-ray luminosity, conversion factor from arcsec to kpc, Largest Angular Size (LAS), previous references to the giant nature and radio image (if available) and finally the radio size (in Mpc).

Soft $\gamma$ -ray Name	Other Name	z	Opt Class	Radio Morph	Log L <sub>14–195 keV</sub> erg/s	Conv Fac kpc/arcsec	LAS arcsec	Ref	Size Mpc
SWIFT J0632.1-5404	QSO J0631-5404	0.2036	Sey1	FR II	44.90	3.314	310	1,a	1.03
SWIFT J0636.5-2036	PKS 0634-20	0.0552	Sy2	FR II	43.80	1.059	900	1,b	0.95
SWIFT J0801.7+4764	RBS 0688	0.1567	Sy1	FR II	44.70	2.682	360	1,c	0.97
B2 1144+35B	RGB J1147+350	0.0631	Sy1.9	FR I	44.15	1.200	710	1,d	0.85
SWIFT J1153.9+5848	RGB J1153+585	0.2024	Sy1.5	FR II	44.99	3.298	255	2,e	0.84
SWIFT J1238.4+5349	RBS 1137	0.3475	Sy1	FR II	45.50	4.884	160	3,f	0.78
SWIFT J1503.7+6850	4C+69.18	0.3180	Sy1.8	FR II	45.41	4.602	190	1,g	0.87
IGR J13107–5626	PMN J1310-5627	0.0930	Sy2	FR II	44.56	1.692	420	2,e	0.71
SWIFT J0225.8+5946	WB J0226+5927	-	-	FR II	-10.99 <sup>†</sup>	-	630	2e	-

<sup>†</sup> Since we are unable to estimate the source luminosity without a knowledge of its redshift, we report for completeness the logarithm value of the 14–195 keV flux (in units of  $\text{erg cm}^{-2} \text{s}^{-1}$ ).

Previous GRG reference: 1) [Kuźmicz et al. \(2018\)](#) 2) this work; 3) [Dabhade et al. \(2020b\)](#), 4) [Bassani et al. \(2016\)](#).

Radio image reference: a) [Saripalli et al. \(2005\)](#); b) [Kronberg et al. \(1986\)](#); c) [Marchā et al. \(2001\)](#); d) [Schoenmakers et al. \(1999\)](#); e) this work; f) [Rafter et al. \(2011\)](#); g) [Lara et al. \(2001\)](#)

### 3 NEWLY DISCOVERED SOURCES

Most of the sources in the sample (see references in Table 1) have already been discussed in the literature: in particular 5 are listed in the catalogue of GRGs by [Kuźmicz et al. \(2018\)](#), while one, SWIFT J1238.4+5349, has recently been reported as a giant in the LOFAR Two-metre Sky Survey (first data release) by [Dabhade et al. \(2020b\)](#). IGR J13107-5626 was suggested as a candidate giant radio galaxy by [Bassani et al. \(2016\)](#), and we can now confirm this initial suggestion. For the remaining object, SWIFT J1153.9+5848, no mention to its large radio structure was found in the literature. Therefore we conclude that two sources in the sample are newly discovered GRGs (SWIFT J1153.9+5848 and IGRJ13107-5626) while one is presented here as a candidate giant radio source (SWIFT J0225.8+5946), waiting for a redshift estimate to confirm its optical class and radio typology. In the following section, each of these three sources will be discussed individually in an attempt to provide further information on their nature.

#### 3.1 SWIFT J1153.9+5848/RGB J1153+585

SWIFT J1153.9+5848 has been associated and classified through this work for the first time; the optical counterpart RGB J1153+585 has mixed classification in NED and SIMBAD, being listed either as a Seyfert 1.5 or a BL Lac. We adopt here the Seyfert classification since the SDSS spectrum shows emission lines and in particular a broad  $H\alpha$  line, all at a redshift of 0.202 (see [Stern & Laor 2012](#) for details of the optical spectrum).

The radio image of the entire source as reported in the NVSS is shown in figure 1 (top left panel): the radio morphology is typical of an FR II galaxy with a bright core marked by the X-ray position and two prominent and fairly symmetric lobes. The NVSS core and total lobe flux densities are 51.8 and 47.6 mJy respectively; the total lobe flux is almost equally divided between the north-eastern (23.3 mJy) and south-western (24.3 mJy) component.

Also shown in figure 1 are zoomed images of each source component (core in the top right panel and individual lobes in the bottom left and right panels) as seen by the VLASS. The core flux density

at 3 GHz<sup>3</sup> is  $37.5 \pm 3.7$  mJy, while that from the north-eastern and south-western lobe is of 4.4 and 13.9 mJy respectively (10% uncertainty). The slight misplacement (2.2'') between X-ray and radio core is perfectly compatible with the X-ray positional uncertainty; the more accurate VLASS position locates the core of this source at RA(J2000)= 11 53 23.92 and Dec(J2000)= +58 31 38.479 (0.5'' uncertainty).

Comparison between NVSS and FIRST surveys indicates that the core flux density is variable over long (yearly) timescale: 51.8 versus 79.4 mJy, respectively ([Abrahamyan et al. 2018](#)). The lobe flux densities measured by FIRST (5.8 and 14.6 mJy for the north-eastern and south-western lobe respectively with a 10% uncertainty) are similar to those of VLASS, implying a flatter spectrum than typically seen in the lobes as expected when probing their most compact and brightest part (i.e. the hot spots visible in figure 1) with high-resolution interferometric observations.

The flux densities provided by NVSS/FIRST and VLASS surveys, allow also to estimate a range of values for the spectral index<sup>4</sup> of the core (-0.42/-0.99), which is clearly influenced by the source variability.

Finally from the flux density values we can also estimate the source radio core dominance, defined here and throughout the paper as  $R = S_{Core}/(S_{Tot} - S_{Core})$ , where  $S_{Core}$  and  $S_{Tot}$  are the core and the total flux densities at a given frequency, respectively. For most of our sources, R can be approximated by the relative core to lobe flux density ratio with the only exception of PKS 0634-20, where the total source emission (estimated to be 8.48 Jy from the NVSS) is twice as large as that of the lobes alone (see section 4.2). The core dominance of SWIFT J1153.9+5848 estimated from the NVSS data is 1.

SWIFT J1153.9+5848 is also listed in the VLBA Imaging and Polarimetry Survey (VIPS, [Helmboldt et al. 2007](#)) where it is reported as a core jet source (jet shorter than 6 mas) with a 5 GHz flux density

<sup>3</sup> VLASS observational bandwidth is 2–4 GHz, so that the middle of this, i.e. 3 GHz, is taken as the reference frequency

<sup>4</sup> Here and in the following, we define the radio spectral index through the expression for flux density as a function of frequency:  $S(\nu) = \nu^\alpha$ .

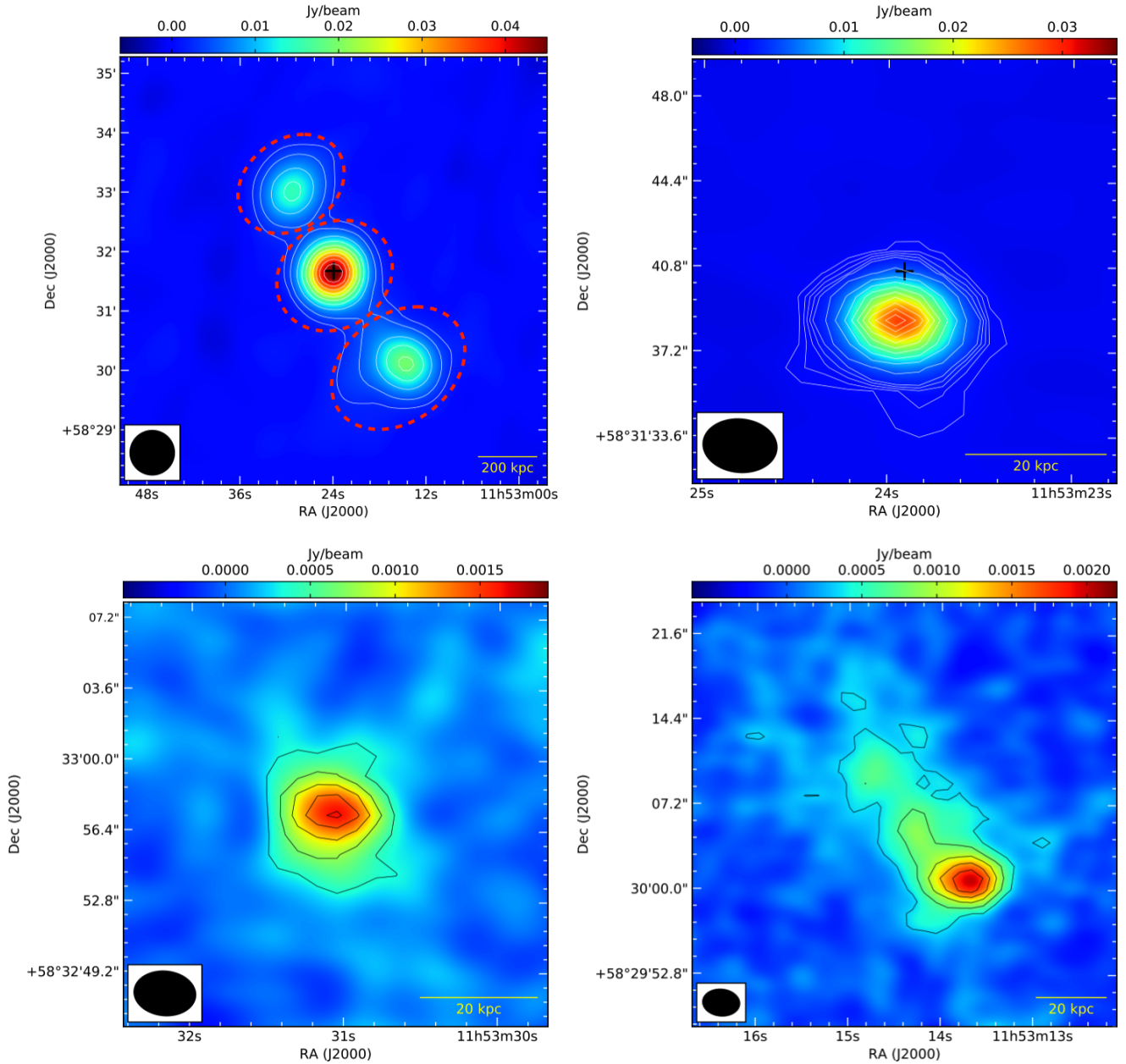


**Figure 1.** Images from NVSS (entire source in the top left panel) and VLASS (core in the top right panel plus north-eastern and south-western lobes in the bottom left and right panel respectively) for SWIFT J1153.9+5848/RGB J1153+585. The NVSS contours are 5,10,20,30,40,50,60,70,80,90% of the source peak flux density which is 46.7mJy/beam. The red dashed regions show the areas used for the flux density extraction. The VLASS contours are 1,2,3,4,5,10,20,30,40,50,60,70,80,90% of the peak flux density which is 35.8 mJy/beam. The black cross in the top figures marks the position of the X-ray core.

of 51.8 mJy. Furthermore, the source is among a set of soft gamma-ray selected GRGs which have LOFAR data and will therefore be the target of a dedicated study (Bruni et al. in preparation).

Beside being core dominated in radio, this GRG is also quite bright at X/soft gamma-ray energies with a 2-10 keV and 14-195 keV luminosities around  $9.4 \times 10^{43}$  erg s $^{-1}$  and  $10^{45}$  erg s $^{-1}$  respectively. If we evaluate the bolometric luminosity, using the correction of Marconi et al. (2004) for the 2-10 keV luminosity (see section 4) we obtain a value of  $3.1 \times 10^{45}$  erg s $^{-1}$ . Assuming instead the relation  $L_{Bol} = 15 \times L_{14-195 \text{ keV}}$ , found by Mushotzky et al. (2008), we obtain a value of  $1.5 \times 10^{46}$  erg s $^{-1}$ . For a black hole mass of  $2.5 \times 10^8$  solar

masses (Greene & Ho 2007), the Eddington luminosity is  $3.2 \times 10^{46}$  erg s $^{-1}$ , implying an Eddington ratio around 0.1 - 0.5, resulting in the most efficient accretor in the current sample of GRGs.

This radio galaxy is also mildly variable at optical wavelength (Abrahamyan et al. 2019); evidence of multi-waveband variability, high core dominance and high accretion rate suggest a blazar like core. Indeed the source is reported as a flat spectrum radio QSO by Sowards-Emmerd et al. (2005) and is also listed in the Rome blazar (BZ) catalogue by Massaro et al. (2009) with the same classification. This blazar like core, which seems very active at the moment, is however embedded in a large double lobe structure which is presumably very

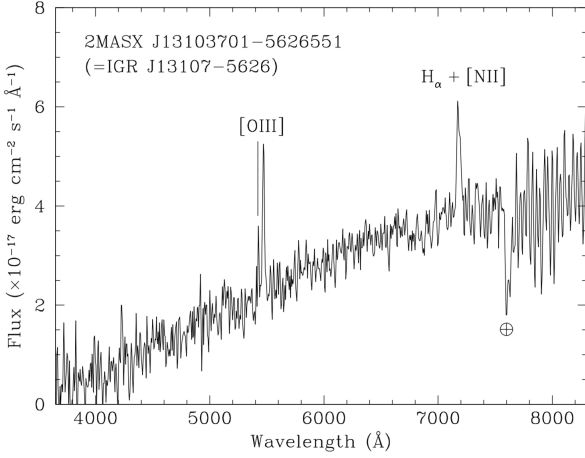


**Figure 2.** Optical spectrum (not corrected for the intervening Galactic absorption) of the counterpart of IGR J13107-5626. The main spectral features are labelled. The symbol  $\oplus$  indicates a telluric absorption band due to atmospheric  $O_2$ .

**Table 2.** Physical properties of the main emission lines in the optical spectrum of the counterpart of IGR J13107-5626. Errors are at  $1\sigma$  confidence level, whereas upper limits are at  $3\sigma$ .

Line	Flux*	$\lambda_{\text{obs}}$	$z$
[O III]	$6.7 \pm 0.7$	$5470 \pm 3$	$0.092 \pm 0.001$
$H_\alpha$	$4.9 \pm 1.0$	$7172 \pm 3$	$0.093 \pm 0.001$
[N II]	$3.3 \pm 0.7$	$7195 \pm 3$	$0.093 \pm 0.001$
$H_\beta$	<1	—	—

\*in units of  $10^{-16} \text{ erg cm}^{-2} \text{ s}^{-1}$

old as indicated by the time it took to reach its current size (around 25 Myr assuming a typical velocity of advancement of 0.1c); thus the source may have restarted activity only recently. Further radio observations at low and high angular scales will shed light on this issue.

### 3.2 IGR J13107-5626/PMN J1310-5627

This source was the only one in Bassani et al. (2016) sample with no redshift, so that it was impossible to estimate the source size at the time of the paper. However the large linear extent of the source suggested a large size, which prompted a follow up study in order to estimate the source distance and optical class; in particular we analyse optical spectra of the source available at the ESO archive (see Appendix B for details of the optical data analysis).

The analysis of the source spectrum (see figure 2) shows the presence of two groups of narrow emission lines superimposed on a reddened (and likely absorbed) continuum; we identify these features as [O III]  $\lambda 5007$  and as the  $H_\alpha + [N II]$  complex at an average common redshift  $z = 0.093 \pm 0.001$ . The physical properties of the main emission lines in the optical spectrum are reported in Table 2.

The relative strengths of [N II] and  $H_\alpha$  (their observed ratio is  $0.67 \pm 0.09$ ), together with the absence of  $H_\beta$ , point to a Type 2 AGN classification for this object, thus securing its identification as the optical counterpart of the high-energy source IGR J13107-5626.

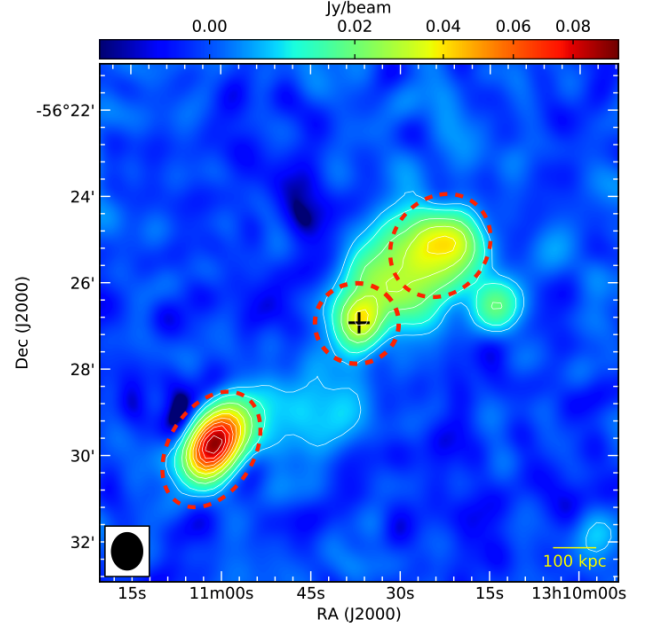


**Figure 3.** SUMSS image of IGR J13107-5626/PMN J1310-5627. It shows the core and two lobes. The SUMSS contours are 5,10,20,30,40,50,60,70,80,90 % of the peak flux density which is 97.3 mJy/beam. The red dashed regions show the areas used for the flux density extraction. The black cross marks the position of the X-ray core.

The source X-ray spectrum is as expected absorbed (see also Landi et al. 2010) and the source 2-10 keV bolometric luminosity is  $3.4 \times 10^{45} \text{ erg s}^{-1}$  using the correction of Marconi et al. (2004); assuming instead the relation of Mushotzky et al. (2008), we obtain a value of  $5.4 \times 10^{45} \text{ erg s}^{-1}$  for the 14-195 keV bolometric luminosity. Unfortunately the black hole mass is not yet available to estimate the source Eddington ratio with some accuracy; however assuming a mass in the range  $10^8 - 10^{10}$  solar masses (as seen in all our GRGs) we obtain Eddington ratios in the range 0.003-0.4.

At radio frequencies the source is poorly studied, but southern surveys provide some useful information. The radio image of PMN J1310-5627 as reported in the SUMSS is shown in figure 3: the radio morphology is typical of an FR II galaxy with a core and two prominent lobes. The radio core which coincides with the X-ray position, is attached to the north-western lobe but it is detached from the south-eastern one; there is some off axis emission south of the core which may be explained as a hydro-dynamical back-flow, i.e. plasma deflected by the host galaxy halo.

The core flux density at 0.8 GHz is 55.6 mJy, while that from the north-western and south-eastern lobe is 82 and 169 mJy respectively (10% uncertainty). This indicates a core dominance of 0.2. The source core is also listed in the catalogue of PMN objects observed with the Australia Telescope Compact Array (McConnell et al. 2012), where it is reported with a 4.8 and 8.6 GHz flux density of 70 and 53 mJy respectively (spectral index -0.5).

This source is poorly studied at all wavelengths but deserves to be the target of a dedicated observational campaign in order to compare its properties, especially in terms of restarting activity, with other GRGs in our sample.

### 3.3 SWIFT J0225.8+5946/WB J0226+5927

Finally SWIFT J0225.8+5946 is a GRG if its redshift exceeds 0.06; unfortunately the source is quite dim at optical wavelengths (B,R magnitudes fainter than 20); indeed it is listed in the Pan-STARRS1 (PS1) catalogue with *i* and *z* magnitudes of 21.63 and 20.66 respectively (Chambers et al. 2016). Therefore a telescope with diameter of at least 3–4 meters is needed to obtain a redshift measurement; for the moment we therefore consider this object as a candidate GRG.

The source WISE colours ( $W1-W2=1.18$ ,  $W2-W3=2.85$ ) indicate that the core of this source is an AGN (Secrest et al. 2015); furthermore these colours suggest that the source may be similar to a blazar of intermediate type between a BL Lac and a FSRQ (D’Abrusco et al. 2014). Interestingly the source is absorbed at X-ray frequencies which may lead to a possible type 2 optical classification.

The source radio image from the NVSS is shown in figure 4 (left panel), where it is evident the large extent of the source and a clear FR II morphology; the core is attached to the north-eastern lobe whereas the south-western one seems to be detached from the rest of the source. The core flux density at 1.4 GHz is 50 mJy, while those from the north-eastern and south-western lobes are of 234 and 94 mJy respectively (10% uncertainty). This indicates a core dominance of 0.15. The source is also listed in the Canadian Galactic Plane Survey (Taylor et al. 2017) with a similar 1.4 GHz core flux density.

Also shown in figure 4 are the VLASS images of the core (middle panel) and north-eastern lobe (right panel) while the south-western one is not detected. The core flux density at 3 GHz is  $58 \pm 9$  mJy while that of the only visible lobe is 48.8 mJy. The more precise positional accuracy of VLASS locates the source core at RA(J2000)= 02 26 25.53 and Dec(J2000)= +59 27 50.933 (uncertainty around 0.5''), only 2.8'' away from the X-ray position.

The source core is also reported in the AMI Galactic plane survey (Perrott et al. 2013) with a 16 GHz flux density of  $61.7 \pm 6.6$  mJy, suggesting a flat spectrum. This again is a poorly studied source, but before performing a more accurate analysis, it is mandatory to obtain a redshift estimate to confirm its GRG nature.

## 4 DISCUSSION

### 4.1 Radio and X-ray properties

To explore further the radio properties of our sources and to compare them with the old GRG sample, we collected from the literature or estimated in this work the radio flux densities and luminosities, mostly relying on high-resolution 0.8–1.4 GHz (SUMSS-NVSS) data that allow to disentangle the different contributions from the core and the lobes. In this way we also were able to estimate the core dominance for all objects. Finally we report when possible the central black hole mass of the AGN. These parameters are all listed in Table 3. The core dominance spans a large range of values from 0.03 to greater than 1, while the black hole masses are also quite high (greater than  $10^8$  solar masses).

Following Ursini et al. (2018) we also compared the X-ray and radio luminosities of the core region, adding 8 new sources to our previous sample of GRGs (see Table 3 and figure 5). As examined in detail by Ursini and co-workers, the major source of uncertainty on the parameters reported in figure 5 is flux variability (which can be roughly of a factor of 2–3), while the measurement errors are relatively small (only a few percent). The Kendall’s correlation coefficient for the whole set of sources is 0.44, with a p-value of  $5e-3$ . For simplicity, to perform the linear fit and compute the correlation we did not take into account PKS 0634–20, for which we only have

an upper limit to the radio core flux density (which is anyway fully compatible with the linear correlation as evident in the figure). With respect to our previous work, the correlation between the two parameters becomes slightly flatter with coefficient  $0.9 \pm 0.2$  instead of  $1.1 \pm 0.3$ , but still within uncertainties (see figure 5). As extensively discussed by Ursini et al. (2018) there are two different branches in the radio–X-ray correlation originally found in X-ray binaries and later extended to AGN: a standard branch with coefficient close to 0.6 and a second one with coefficient in the range 1–1.4. The first branch is consistent with the source being powered by a radiatively inefficient accretion flow while the second one is thought to be associated with a radiatively efficient flow. Therefore a coefficient close to 1 would locate soft gamma-ray selected GRGs on the ‘efficient’ branch of the radio–X-ray correlation diagram, implying a radiatively efficient mode of accretion for these sources.

Following again Ursini et al. (2018), we also calculated two independent estimates of the bolometric luminosity, one from the core X-ray luminosity (which we label  $L_{\text{bol}}^{\text{X}}$ ) and the other from the lobe radio luminosity (which we label  $L_{\text{bol}}^{\text{radio}}$ )

The first estimate,  $L_{\text{bol}}^{\text{X}}$ , is based on the bolometric correction of Marconi et al. (2004) for the 2–10 keV luminosity (see Ursini et al. 2018 for details). As a byproduct of this estimate, we can also evaluate the Eddington ratio  $\lambda_1$ , for all those sources having a measurement of the black hole mass; similarly we estimate the Eddington ratio  $\lambda_2$  using the bolometric correction of Mushotzky et al. (2008) for the 14–195 keV luminosity (see last column of Table 3 for both  $\lambda_1$  and  $\lambda_2$  values). It is evident from the table that most objects are, as indicated by the correlation shown in figure 5, efficient accretors with Eddington ratios above 0.01, with the possible exception of PKS 0634–20 which has a much lower accretion rate ( $3 \times 10^{-4}$ ) based on the 2–10 keV luminosity (but see the considerations made in the next section).

The second estimate of the bolometric luminosity is based on a correlation with the 1.4-GHz lobes luminosity reported by van Velzen et al. (2015), which can be written in the form:

$$\log L_{\text{bol}}^{\text{radio}} = \log L_{1.4\text{GHz}}^{\text{lobes}} + 3.57. \quad (1)$$

Comparison between the above two estimates provides a simple way to relate the AGN activity as traced by the X-ray emission of the nucleus with the one traced by the luminosity of the radio lobes. Because the scatter of the Marconi et al. (2004) relation is  $\sim 0.1$  dex, the main source of uncertainty on  $L_{\text{bol}}^{\text{X}}$  is the X-ray flux variability while that on  $L_{\text{bol}}^{\text{radio}}$  is the scatter of the Van Velzen et al. relation which amounts to 0.3–0.5 dex. Also in this case and despite the uncertainties, we confirm the general trend observed previously that the bolometric luminosity given by the radio lobes is relatively low (around one order of magnitude) compared to the ones given by the nuclear X-ray emission, with only one exception (see figure 6). As discussed by Ursini et al. (2018), this indicates that either the nucleus is now more powerful than in the past, consistent with a restarting of the central engine, or that the giant lobes are dimmer due to expansion losses. The finding that a large fraction of soft gamma-ray-selected GRGs host a young radio nucleus or have indication of multiple activity episodes from their radio morphology (Bruni et al. 2019, 2020) suggests that also for these new objects a scenario of restarting activity is the most likely one.

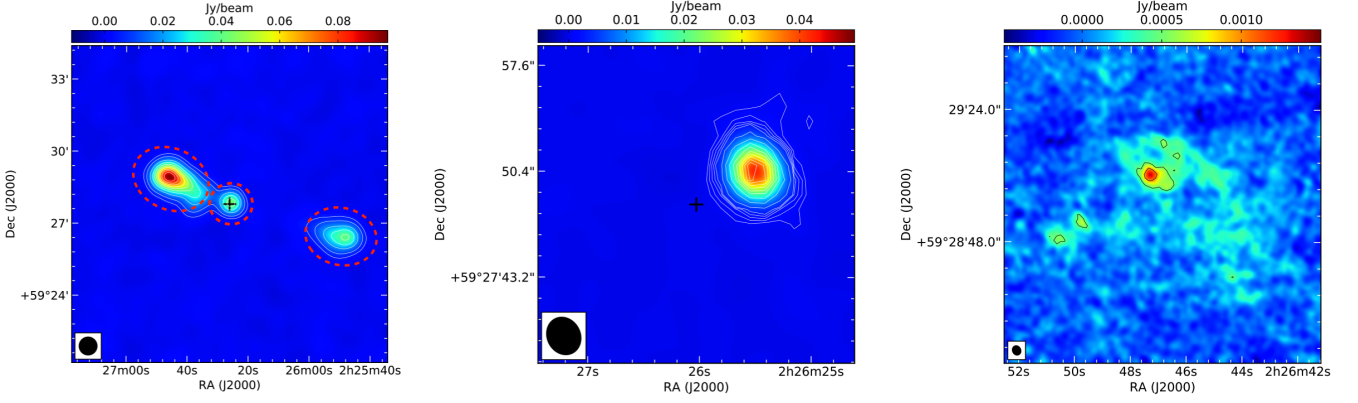


**Figure 4.** Images from NVSS (entire source in the left panel) and VLASS (core in the middle panel plus north-eastern lobe in the right panel) of SWIFT J0225.8+5946/WB J0226+5927. The NVSS contours are 5,10,20,30,40,50,60,70,80,90% of the source peak flux density which is 96.7 mJy/beam. The red dashed regions show the areas used for the flux density extraction. The VLASS contours are 1,2,3,4,5,10,20,30,40,50,60,70,80,90% of the peak flux density which is 49.5 mJy/beam. The black cross in the top left and middle panels marks the position of the X-ray core.

**Table 3.** X-ray and radio properties of the new soft  $\gamma$ -ray selected GRGs. From column 1 to 10 we list the source name from SIMBAD, the core and lobe radio flux densities in mJy, the core and lobe radio luminosities in  $\text{erg s}^{-1}$ , the core dominance R with relative reference, the 2–10 keV X-ray luminosity in  $\text{erg s}^{-1}$ , the log of the black hole mass in solar masses and the Eddington ratios.

Name	$F_{\text{Core}}^{\dagger}$ mJy	$F_{\text{Lobe}}^{\dagger}$ mJy	$L_{\text{Core}}^{\dagger}$ $10^{40} \text{ erg s}^{-1}$	$L_{\text{Lobe}}^{\dagger}$ $10^{41} \text{ erg s}^{-1}$	R (ref)	$L_{2-10\text{keV}}$ $10^{43} \text{ erg s}^{-1}$	$\text{Log} M_{\text{BH, (ref)}}$	$\lambda_1/\lambda_2^{\ddagger}$
QSO J0631-5405 <sup>a</sup>	37.7	< 656	5.17	<8.99	> 0.060, (1)	39.14	9.5, (a)	0.06/0.03
PKS 0634-20	<10.0	3970	<0.1	3.97	<0.001, (2,3)	0.086	8.2, (b)	$3 \times 10^{-4}/0.05$
RBS 0688	57.7	94	5.35	0.87	0.613, (4)	19.85	8.9, (c)	0.09/0.08
RGB J1147+350	340-609	148.4	4.50-8.06	0.20	2.3-4.1, (5)	3.12	8.2, (d)	0.04/0.11
RGB J1153+585	51.8	47.6	8.46	0.78	1.088, (3)	9.35	8.4, (e)	0.1/0.47
RBS 1137	43.2	18.4	24.47	1.04	2.340, (6,7)	15.19	9.7, (c)	0.01/0.07
4C +69.18	88.4	362.6	40.64	16.67	0.244, (8)	91.95	–	–
PMN J1310-5627 <sup>b</sup>	55.6	251	0.95	0.43	0.220(3)	10	–	–
WB J0226+5927	50	328	–	–	0.152, (3)	–	–	–

<sup>†</sup> All radio flux densities are at 1.4GHz, unless otherwise stated

<sup>a</sup> For this source the lobe flux density is given at 0.8GHz; however assuming that lobe spectral indices are generally steep, we can assume this flux density to be also an upper limit to the 1.4 GHz lobe flux density

<sup>b</sup> For this source both core and lobe flux densities are given at 0.8 GHz, consequently the core dominance refer to this frequency.

<sup>‡</sup>  $\lambda_1$  is estimated using the bolometric correction of Marconi et al. (2004) for the 2–10 keV luminosity while  $\lambda_2$  is estimated using the bolometric correction of Mushotzky et al. (2008) for the 14–195 keV luminosity

Core dominance references: 1) Saripalli et al. (2005); 2) Fomalont et al. (2000); 3) this work using NVSS survey for PKS 0634-20, RGB 1153+585 and WB J0226+5927 and SUMSS survey for PMN J1310-5627; 4) Kuźmicz & Jamroz (2012); 5) Schoenmakers et al. (1999); 6) Rafter et al. (2009); 7) Rafter et al. (2011); 8) Lara et al. (2001)

Black hole mass references: a) D’Elia et al. (2003); b) Woo & Urry (2002); c) Brotherton et al. (2015); d) Wu (2009); e) Greene & Ho (2007)

## 4.2 The peculiar case of SWIFT J0636.5-2036/PKS 0634-20

The only exception to the above picture is SWIFT J0636.5-2036/PKS 0634-20, which in figure 6 is located in a region of its own. This location could reflect a wrong estimate either of the X-ray/core bolometric luminosity or of the radio/lobe bolometric one. The first could be due to heavy X-ray obscuration present in the source but not properly accounted for due to the poor quality of the Swift/XRT spectrum: the source is in fact a type 2 AGN and some intrinsic absorption is expected, while the XRT signal to noise ratio is the lowest among the sources analysed here (see Table in Appendix A) are the core and the total flux density. Indeed Simpson et al. (1995) reported strong visual extinction in the source of roughly 30 magnitudes, which im-

plies, for a normal gas to dust ratio<sup>5</sup>, an X-ray column density of at least a few  $10^{22}$  at  $\text{cm}^{-2}$ ; this should be considered as a lower limit as generally extinction in X-rays is stronger than at optical/IR wavelengths. Indeed an old ASCA spectrum of the source, albeit of low signal to noise ratio, indicates that the column density could be as high as  $8 \times 10^{23}$  at  $\text{cm}^{-2}$  (Sambruna et al. 1999) with a consequent large correction (around a factor of 35) to the observed 2-10 keV luminosity reported in Table 3. This correction is close to the value needed to bring the source more in line with all other GRGs indicating that only a heavily absorbed, possibly Compton thick source

<sup>5</sup>  $N_H = A_V/2 \times 10^{21}$  at  $\text{cm}^{-2}$

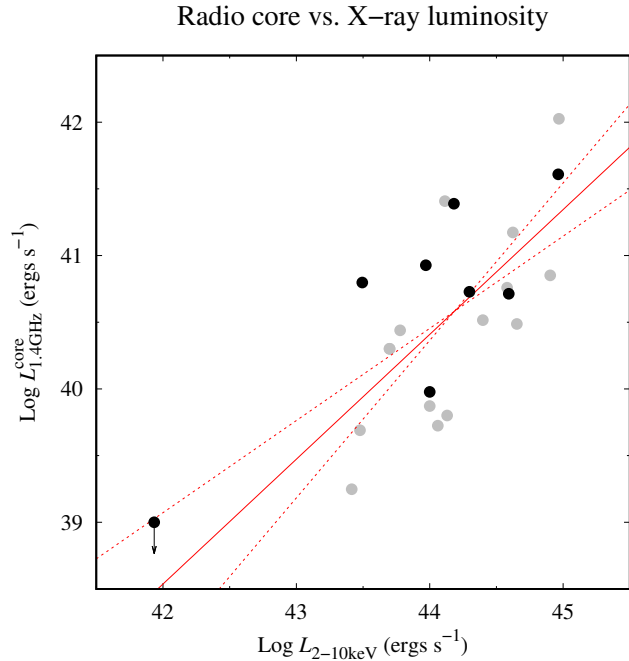


**Figure 5.** Radio core 1.4-GHz luminosity versus X-ray 2–10 keV luminosity. The red solid line represents a linear fit in the log-log space, while the red dashed lines correspond to the 90 per cent error on the slope and normalization. The new GRGs are in black while the old ones are in gray. The only source with an upper limit on the core 1.4-GHz luminosity is PKS 0634-20.

could explain the peculiar location in figure 6. The Compton thick nature of PKS 0634-20 could also be assessed with several diagnostic indicators: for example Bassani et al. (1999) proposed the X-ray/OIII flux ratio while more recently Malizia et al. (2007) proposed the  $F_{2-10keV}/F_{2-100keV}$  softness ratio, where both X-ray fluxes are the observed ones, i.e. not corrected for absorption. In the case of PKS 0634-20 these two diagnostics provide values of 0.33 and 0.02 respectively; both values locate the source in the region populated by Compton thick objects indicating an X-ray column density around  $10^{24}$  at  $\text{cm}^{-2}$ , i.e. not far from the value measured by ASCA. Incidentally heavy intrinsic absorption in X-rays could also alleviate the problem of a low  $\lambda_1$  value while filling at the same time the gap with the much higher  $\lambda_2$  estimate. Only a dedicated long X-ray observation for example combining XMM/NuSTAR pointings can confirm this indication.

Alternatively the radio flux density from the source lobes could be overestimated. The source displays a complex morphology, with a core, two lobes and emission in between (see NVSS image in figure 7, top left panel). The core X-ray position falls in a region of minimum emission so that only an upper limit to the 1.4GHz flux density is available; furthermore between lobes and core a broadened emission region is visible, resembling a plasma back-flow. Separating these various components at the angular resolution available at 1.4GHz is not straightforward and it is possible that the lobe flux density estimated in this work and reported in Table 3 is not perfectly quantified. Indeed the regions used to extract the lobes flux density have been defined in a conservative way, stopping in correspondence of the first minimum of emission found on the lobe-core axis (see red circles in the top left panel of figure 7).

To provide an alternative view at nearby frequencies, we inspected

**Bolometric luminosity from radio vs. X-rays**

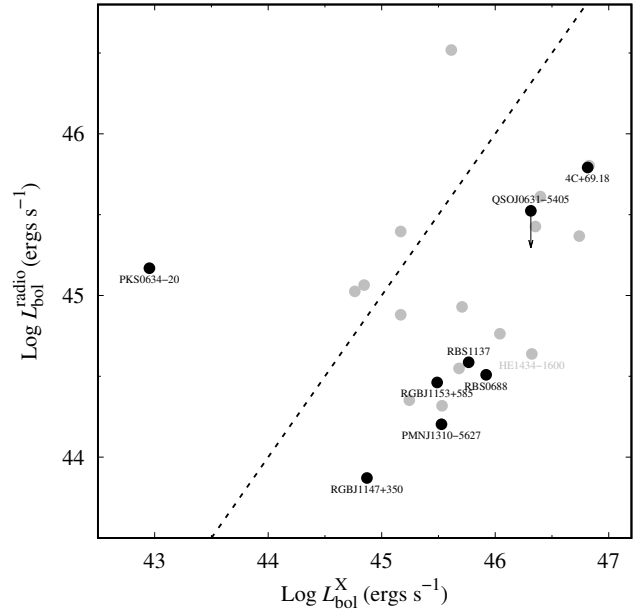


**Figure 6.** Bolometric luminosity estimated from the radio luminosity of the lobes (y axis) versus that estimated from the 2–10 keV luminosity (x axis). The dashed line represents the identity  $y = x$ . The new GRGs are in black while the old ones are in gray. In this figure we also correct a mistake done in Ursini et al. (2018) that caused a wrong placement of HE 1434-1600 (see their Fig. 2).

the VLASS image of the source (see also figure 7) and evaluated the flux density from each component. The more accurate VLASS coordinates locate the source core at RA(J2000)= 06 36 32.21 and Dec(J2000)= -20 34 52.843 (uncertainty  $0.5''$ ), i.e. very close to the X-ray position. The core flux density at 3 GHz is 15 mJy, while that from the northern and southern lobe is of 342 and 1290 mJy respectively (10% uncertainty). The difference between these values and those reported in Table 3 for the lobes (quantified in a factor of  $\sim 2$ ) could be due to many factors. First of all, NVSS and VLASS observations were taken at different frequencies, angular resolution and VLA configurations; moreover it is likely that the oldest electron populations contribute less to the lobe radio emission at higher frequencies, thus providing less flux density in the VLASS. The overall result is that only the most compact emission from the lobe is observed at 3 GHz. To conclude, the NVSS total lobe flux density is, at most, only slightly overestimated.

Taking into account all the above considerations, we conclude that the source position in figure 6 can be moved closer to the line of equality between core and lobes bolometric luminosities (especially if the source is heavily absorbed in X-rays), solving its peculiarity with respect to the other GRGs.

## 5 CONCLUSIONS

A set of new soft gamma-ray selected GRGs has been extracted from recent updates of INTEGRAL/IBIS and Swift/BAT surveys. The set consists of 9 objects, of which 6 were already known, two are discussed here for the first time and one is proposed as a candidate GRG. In the new sample all, but one source, display an FR II radio



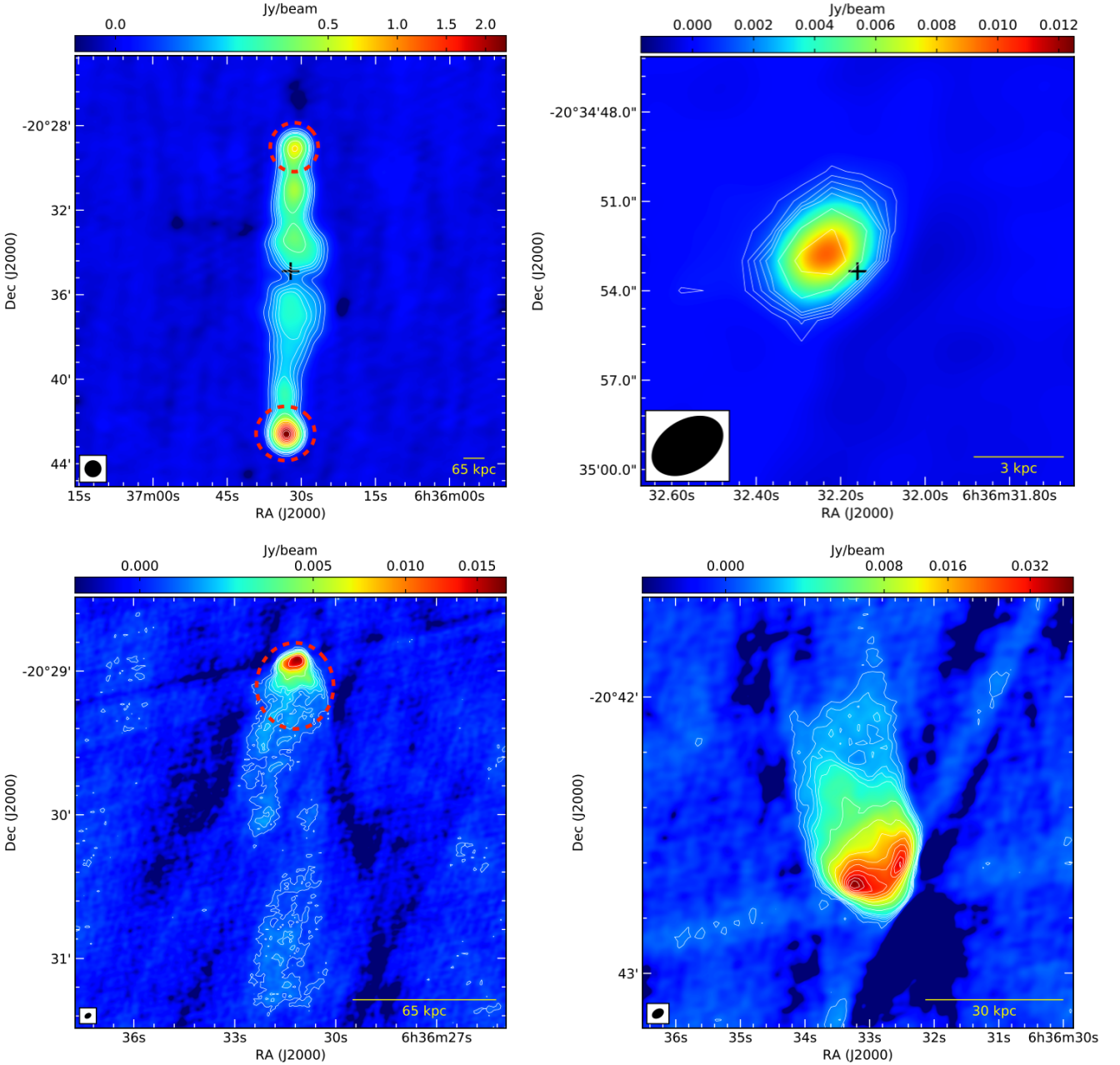


**Figure 7.** Images from NVSS (entire source in the top left panel) and VLASS (core in the top right panel plus north and south lobes in the bottom left and right panel respectively) for SWIFT J0636.5-2036/PKS 0634-20. Contours are 1,2,3,4,5,10,20,30,40,50,60,70,80,90% of the source peak flux density which is 2300 and 43.4 mJy/beam for the NVSS and VLASS respectively. The red dashed regions show the areas used for the flux density extraction. The black cross in the top figures marks the position of the X-ray core.

morphology; the only exception is B21144+35B which is an FR I. The objects belong to both type 1 and 2 AGN optical classes and have redshifts in the range 0.06-0.35, while the radio sizes span from 0.7 to 1 Mpc.

Most of the sources in the sample have already been discussed in the literature except for 3 objects (SWIFT J1153.9+5848/RGB J1153+585, IGR J13107-5626/PMN J1310-5627 and SWIFT J0225.8+5946/WB J0226+5927) which are analysed in more detail here for the first time.

For SWIFT J1153.9+5848/RGB J1153+585 we analyse available radio data, evaluate the flux density of each radio component and

further provide observational evidences which suggest the presence of a blazar like core embedded in the large radio structure.

IGR J13107-5626/PMN J1310-5627 has been optically classified as a type 2/absorbed AGN for the first time in this work; its redshift is 0.093, making this a new GRG (size 0.7 Mpc). We also analyse the SUMSS radio image of the source, estimate the radio flux density of each component, evaluate its core dominance and indicate a possible flat core spectrum.

Finally for SWIFT J0225.8+5946/WB J0226+5927 we find that it is a type 2/absorbed AGN of still unknown redshift. In addition we analyse available radio data and estimate the radio flux density

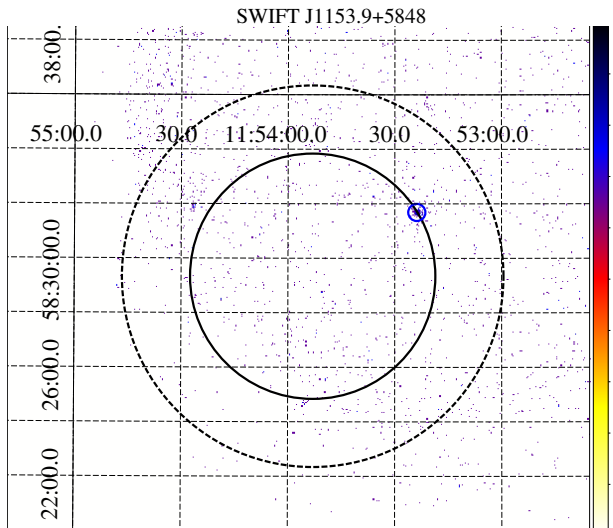


**Figure 8.** XRT image of the SWIFT J1153.9+5848 field, with BAT 90 and 99% error circles.

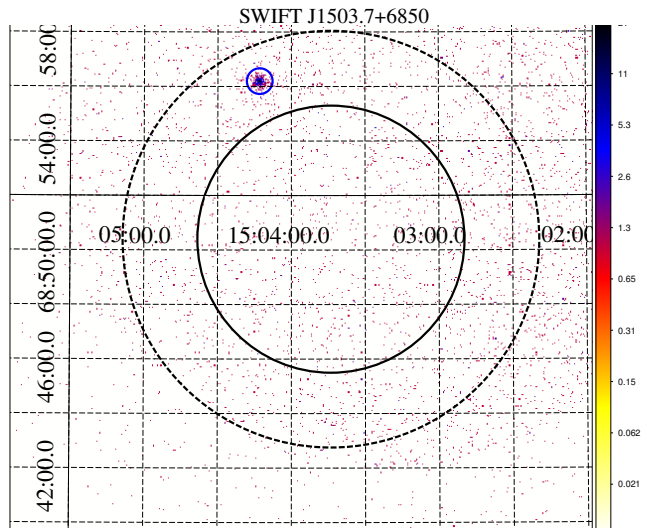


**Figure 9.** XRT image of the SWIFT J1503.7+6850 field, with BAT 90 and 99% error circles.

of each component. The source core dominance is 0.15 and the core spectrum is likely flat.

Also for this set of objects, the X-ray luminosity correlates with the radio core luminosity, as already found by [Ursini et al. \(2018\)](#) for our old sample of GRGs; the correlation follows the ‘efficient’ branch of the radio – X-ray correlation diagram, implying that the soft gamma-ray selection favours the detection of radiatively efficient objects.

Furthermore we confirm that in soft gamma-ray selected GRGs, the radio luminosity of the lobes is relatively low compared with the nuclear luminosity: this can be explained by a significant dimming of the radio lobes due to expansion losses and/or by restarting activity, i.e. the sources are currently highly accreting and in a high luminosity state compared with the past activity that produced the old and extended radio lobes ([Ursini et al. 2018](#)).

The only exception to this picture is PKS 0634-20, which is probably heavily absorbed in X-rays; if a proper correction is applied to the core X-ray luminosity, then the source behaves like other GRGs in the sample.

As already done for our previous set of soft gamma-ray selected GRGs, we intend to follow up each of the sources in the current sample in order to obtain spectral information particularly of the radio core and to study the radio morphology in search of signs of restarting activity.

## APPENDIX A: THE X-RAY DATA ANALYSIS

XRT data, available for 8 GRG, were reduced by means of the XRT-DAS standard data pipeline package (`XRTPIPELINE` v. 0.13.2) to produce screened event files. All data were extracted only in the Photon Counting (PC) mode, since this is the only mode that ensures a source fine positioning.

We stacked together all the available XRT pointings with exposure above 1 ks in order to enhance the signal-to-noise ratio and thus increase source detection probability.

As a following step, we analysed the XRT images in the 0.3–10/3–10 keV energy bands by means of the software package `XIMAGE` v. 4.5.1 in order to substantiate X-ray associations previously reported

in the literature ([Oh et al. 2018](#); [Malizia et al. 2016](#); [Landi et al. 2010](#)) and in the case of SWIFT J1503.7+6850 and SWIFT J1153.9+5848 to search for the most likely soft X-ray counterpart. We confirm all previous associations (X-ray positions and uncertainties as derived by our analysis are reported in Table A1) and also identify the counterpart of the two still unidentified sources.

In each of these two last cases, we find a unique hard X-ray counterpart within the BAT 99% error box (see figure 8 and 9) and report its coordinates and related errors in Table A1; the X-ray positional uncertainty is sufficiently small (few arcsec) to allow the optical association of each source with an active galaxy, RGB J1153+585 for SWIFT J1153.9+5848, and 4C+69.18 for SWIFT J1503.7+6850.

Next, we analysed the spectra of those GRGs for which the quality of the XRT data was good enough to perform a reliable spectral analysis, alternatively only an X-ray flux value has been provided assuming a fixed photon index. Source events were extracted within circular regions, centred on the source position, with a radius in the range 6–20 pixels (1 pixel  $\sim 2.36$  arcsec), chosen depending on the source brightness. Background events were extracted from a source-free region close to the X-ray source of interest. The spectra were obtained from the corresponding event files using the `XSELECT` v. 2.4c software and binned using `GRPPHA` to have at least 1 count per bin, so that the Cash statistic could be applied. We used version v.014 of the response matrices and created individual ancillary response files `arf` using `XRTMKARF` v.0.6.3.

The only source having no XRT coverage (SWIFT J1238.4+5349), was observed by Chandra (see also [Strateva et al. 2008](#)). The Chandra ACIS data were reduced using the package `CIAO` v4.11 and re-processed with the standard tool `CHANDRA_REPRO`. Unfortunately the BAT 90% error circle is only partly covered by the ACIS observation but despite this Chandra detects one source whose coordinates are reported in Table A1. Although we cannot exclude the possibility that other X-ray sources are present within the BAT positional uncertainty, we note that the only source detected is bright enough (its spectral shape extrapolated to the soft gamma-ray band provide a flux similar to the one observed by BAT) to be considered as a highly probable association.

The source spectrum was extracted from a circular region with a radius of 2 arcsec, while the background was extracted from a circular

region with a radius of 20 arcsec. The spectrum was then regrouped with the tool `DMGROUP` to ensure at least 15 counts per bin.

For data fitting of all sources, we adopt a basic model consisting of a simple power law passing through Galactic absorption, unless intrinsic absorption was required as in the case of type 2 AGN. In Table A1, for each GRG observed either by XRT or Chandra, we report total exposure time on source and number of observations considered, the coordinates and relative uncertainties (at 90% c.l.) of the corresponding X-ray counterpart, the count rate in the 0.3–10 keV energy range with relative sigma in parenthesis, and the parameters of the best fit model (photon index and 2-10/0.2-12 keV flux). Comparing with fluxes reported in the XMM-Slew survey (clean catalogue V2.0, Saxton et al. 2008), we note that our XRT fluxes are fully compatible with the range of values reported by XMM for a number of our sources; however the same comparison also indicates some flux variability (a factor of 2-3) on yearly timescale in at least 4 objects (SWIFT J0632.1-5404, SWIFT J0801.7+4764, SWIFT J1238.4+5349 and SWIFT J1503.7+6850).

## APPENDIX B: THE OPTICAL DATA ANALYSIS

We retrieved spectroscopic observations of the optical counterpart of IGR J13107-5626 (see Landi et al. 2010 and Appendix A for the source optical/X-ray coordinates) through the ESO archive<sup>6</sup>. IGR J13107-5626 was observed on 2019 June 19 with the EFOSC2 instrument (Buzzoni et al. 1984), equipped with a Loral/Lesser 2048×2048 pixels CCD, mounted on the 3.58 m New Technology Telescope of the ESO-La Silla Observatory (Chile). Three 1200s exposures were acquired in 2×2 binning mode starting at 01:48 UT with the grism #13 and a 1'' slit: this setup afforded a dispersion of 5.5 Å/pixel.

The observations were bias corrected, flat-fielded, cleaned for cosmic rays, background-subtracted and the corresponding spectra were extracted following standard procedures (Horne 1986) using IRAF<sup>7</sup>.

All calibration frames were acquired on the day preceding the observing night. Wavelength and flux calibrations were performed with the use of lamp acquisitions taken before the science data frames, and of the spectrophotometric standard star LTT 7379 (Hamuy et al. 1992, 1994), respectively. The uncertainty in the wavelength calibration was of 3 Å. All spectra were eventually stacked together to increase the final signal-to-noise ratio.

## ACKNOWLEDGEMENTS

The authors acknowledge financial support from ASI under contract n. 2019-35-HH.0., in particular for G.B. research contract. We thank the anonymous referee for insightful comments and suggestions that improved the quality of the paper.

## DATA AVAILABILITY

The data underlying this article are available in the article. Data not specifically appearing in the article like the products of the X-ray

analysis (spectra and images) will be shared on reasonable request to the corresponding author.

## REFERENCES

- Abrahamyan H. V., Mickaelian A. M., Paronyan G. M., Mikayelyan G. A., Gyulzadyan M. V., 2018, *Astronomy and Computing*, **25**, 176
- Abrahamyan H. V., Mickaelian A. M., Paronyan G. M., Mikayelyan G. A., 2019, *Astronomische Nachrichten*, **340**, 437
- Bassani L., Dadina M., Maiolino R., Salvati M., Risaliti G., Della Ceca R., Matt G., Zamorani G., 1999, *ApJS*, **121**, 473
- Bassani L., Venturi T., Molina M., Malizia A., Dallacasa D., Panessa F., Bazzano A., Ubertini P., 2016, *MNRAS*, **461**, 3165
- Brotherton M. S., Singh V., Runnoe J., 2015, *MNRAS*, **454**, 3864
- Bruni G., et al., 2019, *ApJ*, **875**, 88
- Bruni G., et al., 2020, *MNRAS*, **494**, 902
- Buzzoni B., et al., 1984, *The Messenger*, **38**, 9
- Chambers K. C., et al., 2016, arXiv e-prints, p. arXiv:1612.05560
- Condon J. J., Cotton W. D., Greisen E. W., Yin Q. F., Perley R. A., Taylor G. B., Broderick J. J., 1998, *AJ*, **115**, 1693
- D'Abrusco R., Massaro F., Paggi A., Smith H. A., Masetti N., Landoni M., Tosti G., 2014, *ApJS*, **215**, 14
- D'Elia V., Padovani P., Landt H., 2003, *MNRAS*, **339**, 1081
- Dabhade P., et al., 2020a, arXiv e-prints, p. arXiv:2005.03708
- Dabhade P., et al., 2020b, *A&A*, **635**, A5
- Fanaroff B. L., Riley J. M., 1974, *MNRAS*, **167**, 31P
- Fomalont E. B., Frey S., Paragi Z., Gurvits L. I., Scott W. K., Taylor A. R., Edwards P. G., Hirabayashi H., 2000, *ApJS*, **131**, 95
- Greene J. E., Ho L. C., 2007, *ApJ*, **667**, 131
- Hamuy M., Walker A. R., Suntzeff N. B., Gigoux P., Heathcote S. R., Phillips M. M., 1992, *PASP*, **104**, 533
- Hamuy M., Suntzeff N. B., Heathcote S. R., Walker A. R., Gigoux P., Phillips M. M., 1994, *PASP*, **106**, 566
- Hardcastle M. J., et al., 2019, *MNRAS*, **488**, 3416
- Helmboldt J. F., et al., 2007, *ApJ*, **658**, 203
- Hernández-García L., et al., 2017, *A&A*, **603**, A131
- Horne K., 1986, *PASP*, **98**, 609
- Ishwara-Chandra C. H., Saikia D. J., 1999, *MNRAS*, **309**, 100
- Krivonos R. A., Tsygankov S. S., Mereminskiy I. A., Lutovinov A. A., Sazonov S. Y., Sunyaev R. A., 2017, *MNRAS*, **470**, 512
- Kronberg P. P., Wielebinski R., Graham D. A., 1986, *A&A*, **169**, 63
- Kronberg P. P., Colgate S. A., Li H., Dufton Q. W., 2004, *ApJ*, **604**, L77
- Kuźmicz A., Jamroz M., 2012, *MNRAS*, **426**, 851
- Kuźmicz A., Jamroz M., Bronarska K., Janda-Boczarska K., Saikia D. J., 2018, *ApJS*, **238**, 9
- Lacy M., et al., 2020, *PASP*, **132**, 035001
- Landi R., Bassani L., Malizia A., Stephen J. B., Bazzano A., Focchi M., Bird A. J., 2010, *MNRAS*, **403**, 945
- Lara L., Cotton W. D., Feretti L., Giovannini G., Marcaide J. M., Márquez I., Venturi T., 2001, *A&A*, **370**, 409
- Malarecki J. M., Staveley-Smith L., Saripalli L., Subrahmanyan R., Jones D. H., Duffy A. R., Rioja M., 2013, *MNRAS*, **432**, 200
- Malizia A., et al., 2007, *ApJ*, **668**, 81
- Malizia A., Landi R., Molina M., Bassani L., Bazzano A., Bird A. J., Ubertini P., 2016, *MNRAS*, **460**, 19
- Marchã M. J., Caccianiga A., Browne I. W. A., Jackson N., 2001, *MNRAS*, **326**, 1455
- Marconi A., Risaliti G., Gilli R., Hunt L. K., Maiolino R., Salvati M., 2004, *MNRAS*, **351**, 169
- Massaro E., Giommi P., Leto C., Marchegiani P., Maselli A., Perri M., Piranomonte S., Sclavi S., 2009, *A&A*, **495**, 691
- Mauch T., Murphy T., Battersby H. J., Curran J., Hunstead R. W., Piestrzynski B., Robertson J. G., Sadler E. M., 2003, *MNRAS*, **342**, 1117
- McConnell D., Sadler E. M., Murphy T., Ekers R. D., 2012, *MNRAS*, **422**, 1527
- Mereminskiy I. A., Krivonos R. A., Lutovinov A. A., Sazonov S. Y., Revnivtsev M. G., Sunyaev R. A., 2016, *MNRAS*, **459**, 140

<sup>6</sup> [http://archive.eso.org/eso/eso\\_archive\\_main.html](http://archive.eso.org/eso/eso_archive_main.html)

<sup>7</sup> IRAF is the Image Reduction and Analysis Facility, distributed by the National Optical Astronomy Observatories, which are operated by the Association of Universities for Research in Astronomy, Inc., under cooperative agreement with the National Science Foundation. It is available at <http://iraf.noao.edu>.

**Table A1.** X-ray data analysis of new soft  $\gamma$ -ray selected GRGs

Soft $\gamma$ -ray Name	Instr	Exp (Obs N) Ks	X-ray Position (error) RA(J2000),Dec(J2000),(arcs)	Count rate (sigma) (0.3-10 keV) C/s	$\Gamma$	$F_{2-10keV} / F_{0.2-12keV}$ $10^{-13} \text{ erg cm}^{-2} \text{ s}^{-1}$
SWIFT J0632.1-5404	XRT	1.6 (1)	06 32 00.95,-54 04 55.89 (3.8)	152.3±9.7 (15.7)	1.92± 0.15	40±10 /78±10
SWIFT J0636.5-2036	XRT	22.5 (7)	06 36 32.16,-20 34 53.35 (4.1)	2.2±0.3 (7.3)	1.70± 0.4	1.2±0.4 /1.8±0.6
SWIFT J0801.7+4764	XRT	7.7 (1)	08 01 31.96,+47 36 15.43 (3.6)	145.9±4.6 (31.7)	2.05± 0.08	30±3 /65±4
B2 1144+35B	XRT	4.7 (1)	11 47 22.52,+35 01 08.55 (3.7)	82.2±4.2 (19.6)	1.58± 0.12	33±5 /55±7
SWIFT J1153.9+5848(U3)	XRT	5.9 (4)	11 53 23.91,+58 31 40.65 (3.9)	23.0±2.0 (11.5)	1.60± 0.2	8±2 /14±3
SWIFT J1238.4+5349	Chandra	4.9 (1)	12 38 07.77,+53 25 55.99 (1.0)	284.0±8.0 (35.5)	1.79± 0.09	13±2 /24±2
SWIFT J1503.7+6850(U1)	XRT	4.1 (3)	15 04 13.11,+68 56 11.63 (3.7)	100.0±5.0 (20.0)	1.63± 0.2	28±5 /51±6
IGR J13107-5626	XRT	6.6 (1)	13 10 36.90,-56 26 56.31 (4.9)	5.5±0.9 (6.1)	1.8f	14±5 /21±7
SWIFT J0225.8+5946	XRT	1.5 (1)	02 26 26.03,+59 27 48.15 (5.4)	16.0±3.0 (5.3) -	1.8f	2±1/3±2

In IGR J13107–5626 an intrinsic column density of  $(3_{-1}^{+3}) \times 10^{23}$  at  $\text{cm}^{-2}$  is present;

In SWIFT J0225.8+5946 an intrinsic column density  $(3_{-2}^{+3}) \times 10^{22}$  at  $\text{cm}^{-2}$  is present.

- Mushotzky R. F., Winter L. M., McIntosh D. H., Tueller J., 2008, *ApJ*, **684**, L65
- Oh K., et al., 2018, *ApJS*, **235**, 4
- Perrott Y. C., et al., 2013, *MNRAS*, **429**, 3330
- Rafter S. E., Crenshaw D. M., Wiita P. J., 2009, *AJ*, **137**, 42
- Rafter S. E., Crenshaw D. M., Wiita P. J., 2011, *AJ*, **141**, 85
- Sambruna R. M., Eracleous M., Mushotzky R. F., 1999, *ApJ*, **526**, 60
- Saripalli L., Hunstead R. W., Subrahmanyan R., Boyce E., 2005, *AJ*, **130**, 896
- Saxton R. D., Read A. M., Esquej P., Freyberg M. J., Altieri B., Bermejo D., 2008, VizieR Online Data Catalog, [pp J/A+A/480/611](#)
- Schoenmakers A. P., de Bruyn A. G., Röttgering H. J. A., van der Laan H., 1999, *A&A*, **341**, 44
- Secrest N. J., Dudik R. P., Dorland B. N., Zacharias N., Makarov V., Fey A., Frouard J., Finch C., 2015, *ApJS*, **221**, 12
- Simpson C., Ward M. J., Wilson A. S., 1995, *ApJ*, **454**, 683
- Sowards-Emmerd D., Romani R. W., Michelson P. F., Healey S. E., Nolan P. L., 2005, *ApJ*, **626**, 95
- Stern J., Laor A., 2012, *MNRAS*, **423**, 600
- Strateva I. V., Brandt W. N., Eracleous M., Garmire G., 2008, *ApJ*, **687**, 869
- Stuardi C., et al., 2020, arXiv e-prints, [p. arXiv:2004.05169](#)
- Taylor A. R., Leahy D. A., Tian W. W., Sunstrum C., Kothes R., Landecker T. L., Ransom R. R., Higgs L. A., 2017, *AJ*, **153**, 113
- Ursini F., et al., 2018, *MNRAS*, **481**, 4250
- White R. L., Becker R. H., Helfand D. J., Gregg M. D., 1997, *ApJ*, **475**, 479
- Woo J.-H., Urry C. M., 2002, *ApJ*, **579**, 530
- Wu Q., 2009, *MNRAS*, **398**, 1905
- van Velzen S., Falcke H., Körding E., 2015, *MNRAS*, **446**, 2985